12-21-2021

Cross Talk between ARF1 and RhoA Coordinates the Formation of Cytoskeletal Scaffolds during Chlamydia Infection

Adam Haines
Thomas Jefferson University

Jordan Wesolowski
Thomas Jefferson University

Nathan M Ryan
Thomas Jefferson University

Tiago Monteiro-Brás
Thomas Jefferson University

Fabienne Paumet
Thomas Jefferson University

AMERICAN SOCIETY FOR MICROBIOLOGY | mBio®

RESEARCH ARTICLE

Cross Talk between ARF1 and RhoA Coordinates the Formation of Cytoskeletal Scaffolds during *Chlamydia* Infection

Adam Haines,[a] Jordan Wesolowski,[a] Nathan M. Ryan,[a] Tiago Monteiro-Brás,[a,b,c] Fabienne Paumet[a]

[a]Department of Immunology and Microbiology, Thomas Jefferson University, Philadelphia, Pennsylvania, USA
[b]Life and Health Sciences Research Institute (ICVS), School of Medicine, University of Minho, Braga, Portugal
[c]ICVS/3B's, PT Government Associate Laboratory, Braga/Guimarães, Portugal

Adam Haines and Jordan Wesolowski contributed equally to this article. Author order was determined alphabetically.

ABSTRACT *Chlamydia trachomatis* is an obligate intracellular bacterium that has developed sophisticated mechanisms to survive inside its infectious compartment, the inclusion. Notably, *Chlamydia* weaves an extensive network of microtubules (MTs) and actin filaments to enable interactions with host organelles and enhance its stability. Despite the global health and economic burden caused by this sexually transmitted pathogen, little is known about how actin and MT scaffolds are integrated into an increasingly complex virulence system. Previously, we established that the chlamydial effector InaC interacts with ARF1 to stabilize MTs. We now demonstrate that InaC regulates RhoA to control actin scaffolds. InaC relies on cross talk between ARF1 and RhoA to coordinate MTs and actin, where the presence of RhoA downregulates stable MT scaffolds and ARF1 activation inhibits actin scaffolds. Understanding how *Chlamydia* hijacks complex networks will help elucidate how this clinically significant pathogen parasitizes its host and reveal novel cellular signaling pathways.

IMPORTANCE *Chlamydia trachomatis* is a major cause of human disease worldwide. The ability of *Chlamydia* to establish infection and cause disease depends on the maintenance of its parasitic niche, called the inclusion. To accomplish this feat, *Chlamydia* reorganizes host actin and microtubules around the inclusion membrane. How *Chlamydia* orchestrates these complex processes, however, is largely unknown. Here, we discovered that the chlamydial effector InaC activates Ras homolog family member A (RhoA) to control the formation of actin scaffolds around the inclusion, an event that is critical for inclusion stability. Furthermore, InaC directs the kinetics of actin and posttranslationally modified microtubule scaffolds by mediating cross talk between the GTPases that control these cytoskeletal elements, RhoA and ADP-ribosylation factor 1 (ARF1). The precise timing of these events is essential for the maintenance of the inclusion. Overall, this study provides the first evidence of ARF1-RhoA-mediated cross talk by a bacterial pathogen to coopt the host cytoskeleton.

KEYWORDS ARF1, *Chlamydia*, GTPases, RhoA, actin, cytoskeleton, microtubules

Actin and tubulin are among the most abundant proteins in eukaryotic cells and are involved in essential cellular processes, including organelle positioning and function. Together, they comprise the most critical components in the cytoskeleton: actin filaments and microtubules (MTs). Additional cellular proteins regulate each cytoskeletal element's structure, dynamics, and function and, consequently, the fundamental biological processes dependent on the cytoskeleton (1). As a result, these regulatory components of the cytoskeleton are significant targets for intracellular bacterial pathogens (2–4).

Editor Craig R. Roy, Yale University School of Medicine

Address correspondence to Fabienne Paumet, fabienne.paumet@jefferson.edu.

The authors declare no conflict of interest.

Received 10 August 2021
Accepted 4 November 2021
Published 14 December 2021

Chlamydia trachomatis is the most common cause of bacterial sexually transmitted disease. It is also the most frequent cause of infectious blindness, known as trachoma (5). *C. trachomatis* displays a unique biphasic lifestyle. The infectious form, called the elementary body (EB), exhibits minimal metabolic activity and promotes its entry into human epithelial cells. Once inside the host cell, *Chlamydia* EBs reside within a membrane-bound compartment called the inclusion. EBs then rapidly differentiate into a replicative form, called the reticulate body (RB), which is metabolically active and noninfectious. As RBs replicate by binary fission, they synthesize effector proteins that remodel and hijack the host cell to promote their survival (6). In doing so, *Chlamydia* subverts many aspects of the host cellular environment, including the host cytoskeleton, a critical element of successful infection and dissemination of *C. trachomatis* within the host.

EBs initially invade the host cell by attaching to the plasma membrane and injecting the chlamydial protein Tarp (translocated actin recruiting protein) into the host cytoplasm via the chlamydial type III secretion system. Phosphorylation of Tarp in the cytosol allows Tarp to recruit the guanine nucleotide exchange factors (GEFs) Sos1 and Vav2, which activate Rac1 (7). Tarp directly binds actin monomers to nucleate new linear filaments (8, 9). Subsequently, the Arp2/3 complex is activated, and branched actin filaments are polymerized underneath the bacterial binding site to promote the entry of the EBs into the nascent inclusion (10–12).

The second wave of cytoskeletal manipulation begins around 16 h postinfection (hpi), when MTs are assembled around the inclusion (13). These scaffolds are subsequently stabilized and undergo posttranslational modification (PTM), including detyrosination and acetylation (14, 15). PTMs influence MT structure and depolymerization rates, further increasing their stability (16, 17). We have previously established that the small GTPase ARF1 controls the posttranslational modification of MT scaffolds. PTM-MT scaffolds then position Golgi ministacks around the inclusion, which provides lipids to facilitate the rapid expansion of the inclusion (14, 15, 18). Around 32 hpi, actin scaffolds form around the inclusion. These structures physically reinforce the inclusion membrane to prevent premature lysis, as the inclusion expands to occupy most of the host cytoplasm (19). Using actin-depolymerizing agents and small interfering RNA (siRNA), the formation of F-actin at the inclusion was shown to be RhoA dependent (19).

Finally, *Chlamydia* exits its host cell either by controlled cell lysis or through extrusion, which also relies on the intervention of the host cytoskeleton. Extrusion is a nonlytic process during which the inclusion protrudes out of the infected cell before pinching off the plasma membrane (20). This event requires the mobilization of RhoA, WASP, and myosin II. Interestingly, MT depolymerization with nocodazole does not affect extrusion, suggesting this event is actin specific (20).

Interference with the host cytoskeleton dramatically impacts the outcome of *Chlamydia* infection. The inhibition of PTM-MT scaffolds decreases *Chlamydia* infectivity, whereas their enhancement increases it, demonstrating the importance of this cytoskeletal element in *Chlamydia* development (14). Global inhibition of actin polymerization with latrunculin also causes early rupture of inclusions, indicating that actin is essential for maintaining inclusion stability (19). Inclusion stability solely depends on actin, as MT depolymerization does not impact inclusion integrity (19).

Previous work investigating *Chlamydia* has been significantly limited by its reliance on cytoskeleton-modulating drugs. These drugs disrupt the host cytoskeleton in its entirety and often indirectly impact other cytoskeletal elements (21). As a result, elucidating the precise local role of actin and MT scaffolds during *Chlamydia* infection has been challenging. However, with advances in *Chlamydia* genetics, targeted disruption of *Chlamydia*'s virulence system and its effector proteins is now possible without indirectly affecting native host processes. Recently, we and others showed that a single chlamydial effector, InaC (also called CT813 or CTL0184), controls the formation of the kinetically and functionally distinct actin and PTM-MT scaffolds (15, 19, 22). InaC knockout (KO) *Chlamydia* produces less-infectious progeny and generates smaller inclusions,

indicating that InaC-dependent pathways are essential for *Chlamydia* fitness (15, 19). We also demonstrated that InaC directly interacts with the host small GTPases ARF1 and ARF4 to control the formation of PTM-MTs and, consequently, the dispersal of Golgi ministacks around the inclusion during infection (15). This event occurs midcycle at 16 to 24 hpi. In addition to InaC, it has been shown that actin scaffold formation around 32 hpi is mainly dependent on the host GTPase RhoA (19). Whether InaC regulates RhoA and how both GTPases are coordinated during infection to generate their specific scaffolds at the optimal time is unknown.

Here, we report that while RhoA can be recruited to the inclusion in the absence of InaC, its activation, which leads to the formation of actin scaffolds, requires InaC. Furthermore, we discovered that the presence of RhoA downregulates ARF1 activation, while ARF1-GTP inhibits RhoA activation, highlighting cross talk between two small GTPases to coordinate PTM-MT and actin scaffolds during infection. Overall, our findings establish that a single chlamydial effector, InaC, is a master regulator of actin and MT dynamics during *Chlamydia* infection.

RESULTS

RhoA activation is required for the formation of actin scaffolds around the inclusion. To understand the exact role of RhoA during *C. trachomatis* infection and to assess whether RhoA is the sole regulator of actin scaffold formation, we generated CRISPR/Cas9 RhoA KO HeLa cells (see Fig. S1A in the supplemental material). HeLa cells transfected with the Cas9 vector without guide RNA were used as a control. RhoA KO cells also express similar amounts of actin, α-tubulin, and acetylated α-tubulin compared to control cells (Fig. S1B). We detected a modest but statistically insignificant increase in detyrosinated α-tubulin in the absence of RhoA. As expected, RhoA KO cells are viable and divide similarly to control cells (Fig. S1C and D).

Next, we assessed the kinetics of actin scaffold formation in the presence and absence of RhoA during *Chlamydia* infection. Control and RhoA KO cells were infected with wild-type (WT) *C. trachomatis* L2 prior to the analysis of actin scaffolds around the inclusion at different times postinfection. In parallel, RhoA KO cells were transfected with a vector encoding myc-RhoA$_{WT}$ (RhoA$_{WT}$) at 3 to 4 hpi to restore RhoA expression. In control cells, actin scaffolds are detected at 38 hpi, but not 24 hpi (Fig. 1A and B, Control), consistent with previous observations that actin scaffolds form late during infection (19). In contrast, actin scaffolds were not detectable at either time point in RhoA KO cells (Fig. 1A and B, RhoA KO). The expression of myc-RhoA$_{WT}$ rescued the loss of actin scaffolds in RhoA KO cells at 38 hpi (Fig. 1B, RhoA$_{WT}$), indicating that the loss of actin scaffolds in RhoA KO cells is not due to an off-target effect of Cas9.

Like all small GTPases, RhoA cycles between GDP- and GTP-bound states, which in turn control its interactions with downstream effectors (23). To assess whether *Chlamydia* infection influences the activation state of RhoA to promote actin polymerization around the inclusion, we infected HeLa cells with *C. trachomatis* L2 and generated lysates from mid to late times postinfection (16 to 48 hpi). The levels of RhoA-GTP were then analyzed using the RhoA-binding domain (RBD) of the effector Rhotekin (24). The activation of RhoA reaches a maximal level at 32 hpi (Fig. 1C), which correlates with both the formation of actin scaffolds and the recruitment of endogenous RhoA to the inclusion (Fig. S2). Note that RhoA activation is a transient event, as it is deactivated and returns to noninfected levels at ~40 hpi. These data indicate that *C. trachomatis* triggers the activation of RhoA at the same time that actin polymerization occurs around the inclusion.

To establish the role of RhoA activation in the formation of actin scaffolds, we exploited the well-characterized G14V (myc-RhoA$_{G14V}$, GTP locked) and T19N (myc-RhoA$_{T19N}$, dominant negative) RhoA mutants, which have been used extensively to explore the biological activities of RhoA (25–27). At 3 to 4 hpi with *C. trachomatis* L2, we transfected RhoA KO cells with either myc-RhoA$_{G14V}$ or myc-RhoA$_{T19N}$ and compared the formation of actin scaffolds to that of cells transfected with myc-RhoA$_{WT}$. We found that myc-RhoA$_{G14V}$, but not myc-RhoA$_{T19N}$, supports actin scaffold formation (Fig. 1D).

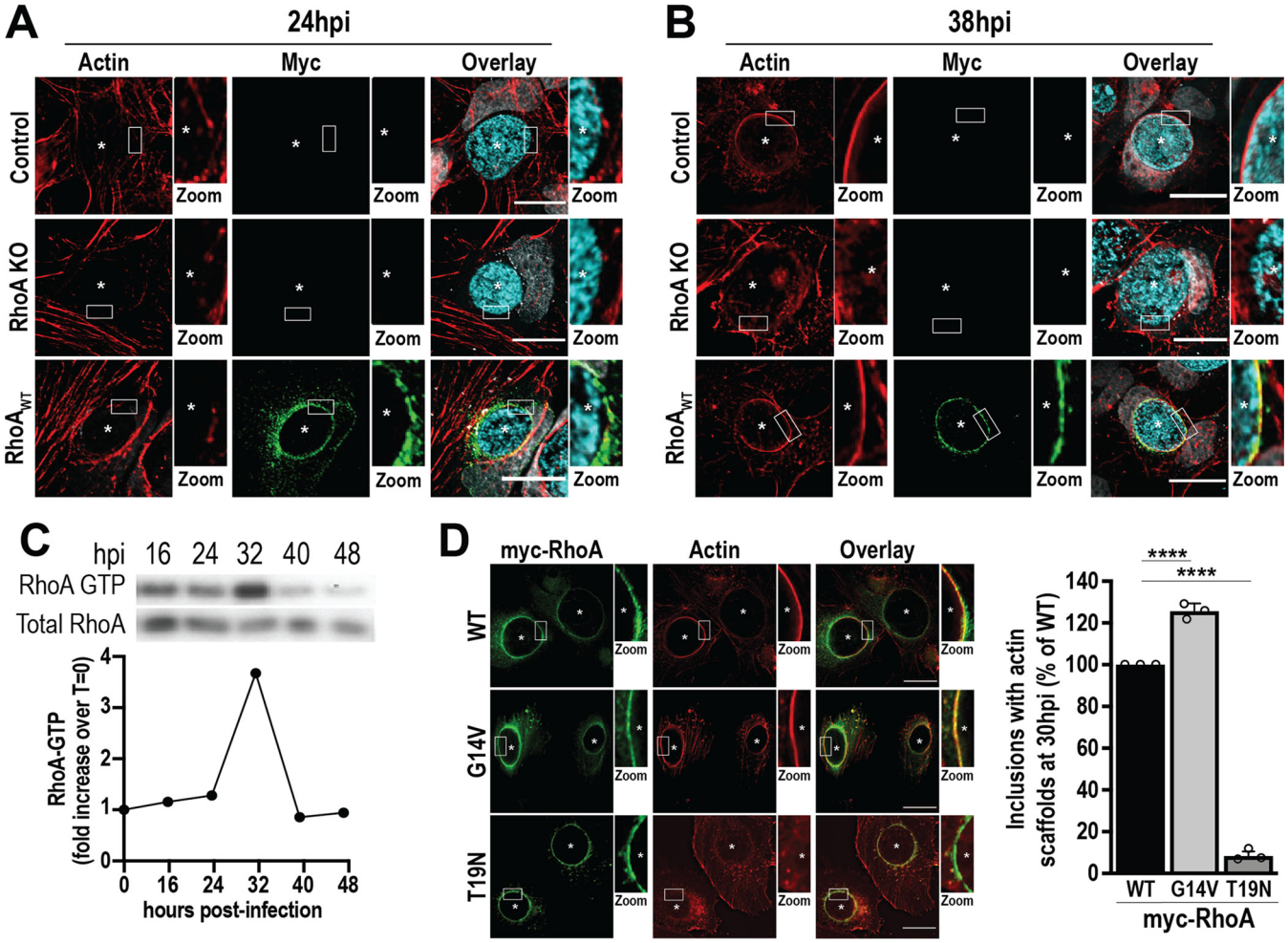

FIG 1 Active RhoA is required for the formation of actin scaffolds around the inclusion. (A and B) Control and RhoA KO cells were infected with WT *C. trachomatis* L2 (MOI of 2) and transfected with empty or myc-RhoA$_{WT}$ DNA at 4 hpi. Cells were fixed at 24 or 38 hpi and labeled with phalloidin to label actin (red), anti-myc antibody to label RhoA (green), and anti-MOMP antibody to label individual *Chlamydia* (cyan). Asterisks denote inclusions. The white box indicates the magnified area shown to the right of the image (Zoom). Images are representative of 3 independent experiments. Scale bar, 25 μm. (C) HeLa cells were infected with WT *C. trachomatis* L2 (MOI of 1) for the indicated times prior to lysis and isolation of RhoA-GTP using the RhoA binding domain of Rhotekin immobilized on agarose beads. In the Western blot, RhoA-GTP denotes the RhoA signal from the pulldown, and Total RhoA represents the amount of RhoA from the cell lysate. The graph indicates the fold increase in RhoA-GTP compared to a noninfected control (t = 0). Results are representative of two independent experiments. (D) RhoA KO cells were infected with WT *C. trachomatis* L2 (MOI of 2) and transfected with myc-RhoA$_{WT}$, myc-RhoA$_{G14V}$, or myc-RhoA$_{T19N}$ DNA at 4 hpi. Cells were fixed 30 hpi and labeled with anti-myc (green) antibody and phalloidin (red). Scale bar, 20 μm. Asterisks denote inclusions. The white box indicates the magnified area shown to the right of the image (Zoom). The graph denotes the average percentage of inclusions containing actin scaffolds from 3 independent experiments ± the standard deviation. Data are normalized to myc-RhoA$_{WT}$-expressing cells. A minimum of 100 inclusions was counted for each condition per experiment. ****, $P < 0.0001$.

Compared to infected myc-RhoA$_{WT}$-expressing cells, the expression of myc-RhoA$_{G14V}$ maximizes actin scaffold formation to 126% ± 3.7%. In comparison, only 9% ± 2.1% of inclusions displayed actin scaffolds in RhoA$_{T19N}$-expressing cells, demonstrating that active RhoA is required to promote actin scaffold formation. Interestingly, actin scaffolds become detectable at 24 hpi in cells expressing constitutively active myc-RhoA$_{G14V}$, while they are absent in cells expressing myc-RhoA$_{WT}$ and myc-RhoA$_{T19N}$ (see Fig. S3 in the supplemental material). In this case, we observe that 86% ± 4.2% of inclusions have actin scaffolds as early as 24 hpi. This is not due to a shift in RhoA recruitment since endogenous RhoA is already present on the inclusion at 24 hpi (Fig. S2) despite the absence of actin scaffolds (Fig. 1A). Altogether, these data indicate that the temporal activation of RhoA is critical and dictates the kinetics of actin scaffold formation during infection.

The chlamydial effector InaC is required for the activation of RhoA. InaC is a chlamydial effector that is required for the formation of actin scaffolds during

Chlamydia infection (15, 19). To establish whether InaC regulates the activity of RhoA during infection, we made use of a *C. trachomatis* L2 mutant in which the InaC gene was inactivated using Targetron (InaC KO *Chlamydia*) (15). We then infected HeLa cells with InaC KO *C. trachomatis* L2 and quantified the amount of RhoA-GTP at 32 hpi. Infection with WT *C. trachomatis* L2 increased RhoA-GTP levels 2.9 ± 0.54-fold compared to uninfected control cells (Fig. 2A). In contrast, InaC KO-infected cells exhibited RhoA-GTP levels similar to control cells (0.983 ± 0.34-fold change), indicating that InaC is required in RhoA activation during *C. trachomatis* infection.

One way that proteins regulate each other is through direct interactions. We thus tested whether InaC forms a complex with RhoA to control its activation locally. To do so, we conducted a series of immunoprecipitation experiments in the presence and absence of infection in different configurations. However, we could not detect an interaction (see Fig. S4 in the supplemental material), indicating that either InaC and RhoA do not bind or the interaction is too weak or transient to detect.

Even though InaC and RhoA do not form a detectable complex, the recruitment of RhoA to the inclusion could still be indirectly impacted by the absence of InaC, which would explain the reduction in RhoA-GTP in cells infected with InaC KO *C. trachomatis* L2 (Fig. 2A). To assess whether RhoA recruitment to the inclusion depends on InaC, we used RhoA KO cells complemented with myc-$RhoA_{WT}$ and infected with WT or InaC KO *C. trachomatis* L2. At 32 to 38 hpi, infected cells were fixed and stained with anti-myc and anti-InaC antibodies to label RhoA and the inclusion membrane, respectively. As expected, myc-$RhoA_{WT}$ was present on the inclusion membrane in WT *C. trachomatis* L2-infected cells (Fig. 2B, WT L2). Interestingly, myc-$RhoA_{WT}$ was also detected on the inclusion membrane of InaC KO *C. trachomatis* L2-infected cells (Fig. 2B, InaC KO), indicating that RhoA recruitment is InaC independent. Next, we assessed whether both mutant forms of RhoA are differentially recruited during infection with InaC KO *Chlamydia*. As shown in Fig. 2C and D, myc-$RhoA_{G14V}$ (Fig. 2C) and myc-$RhoA_{T19N}$ (Fig. 2D) are also recruited to the inclusion in both WT and InaC KO *C. trachomatis* L2-infected cells. These data further indicate that RhoA is recruited to the inclusion independently of its activation state.

We then determined whether the loss of actin scaffolds in InaC KO *C. trachomatis* L2-infected cells is due to a defect in RhoA activation. To do so, we infected RhoA KO HeLa cells with WT or InaC KO *C. trachomatis* L2, followed by transfection with myc-$RhoA_{WT}$, myc-$RhoA_{G14V}$, or myc-$RhoA_{T19N}$ DNA. The cells were fixed at 32 to 38 hpi and labeled with anti-myc and anti-InaC antibodies. As observed earlier, myc-$RhoA_{WT}$ and myc-$RhoA_{G14V}$, but not myc-$RhoA_{T19N}$, promote the formation of actin scaffolds during WT *C. trachomatis* infection (Fig. 2B to E, WT L2). Strikingly, the expression of myc-$RhoA_{G14V}$, but not myc-$RhoA_{WT}$ or myc-$RhoA_{T19N}$, rescues the InaC KO phenotype and fully restores the formation of actin scaffolds (Fig. 2B to E, InaC KO), indicating that the loss of actin scaffolds in InaC KO-infected cells is due to an inability to activate RhoA. Altogether, these results demonstrate that InaC is not required to recruit RhoA but rather to locally activate it and promote actin scaffold formation around the inclusion. Since RhoA does not interact with InaC, it is likely that an additional host or bacterial factor that remains to be identified is involved.

InaC-RhoA-mediated cytoskeletal scaffolds contribute to inclusion stability. InaC is required for the formation of both PTM-MT and actin scaffolds (15, 22). However, their direct contribution to inclusion stability is not well understood. To test the importance of these scaffolds in *Chlamydia* fitness, we infected HeLa cells with InaC KO *C. trachomatis* L2 and assessed inclusion stability over time. In WT *C. trachomatis* L2-infected cells, we observed that ~40% of inclusions were ruptured at 48 hpi. In contrast, ~50% of the InaC KO inclusions were lysed by 32 hpi (Fig. 3A), indicating a substantial shift in inclusion stability in the absence of InaC. This early release of *Chlamydia* into the cytosol correlated with a 2.4-fold increase in cell death measured by caspase 3/7 activation. While only 5% ± 0.98% of WT *C. trachomatis* L2-infected cells were positive for caspase 3/7 activation, 12% ± 0.86% of InaC KO *C. trachomatis* L2-infected cells were positive

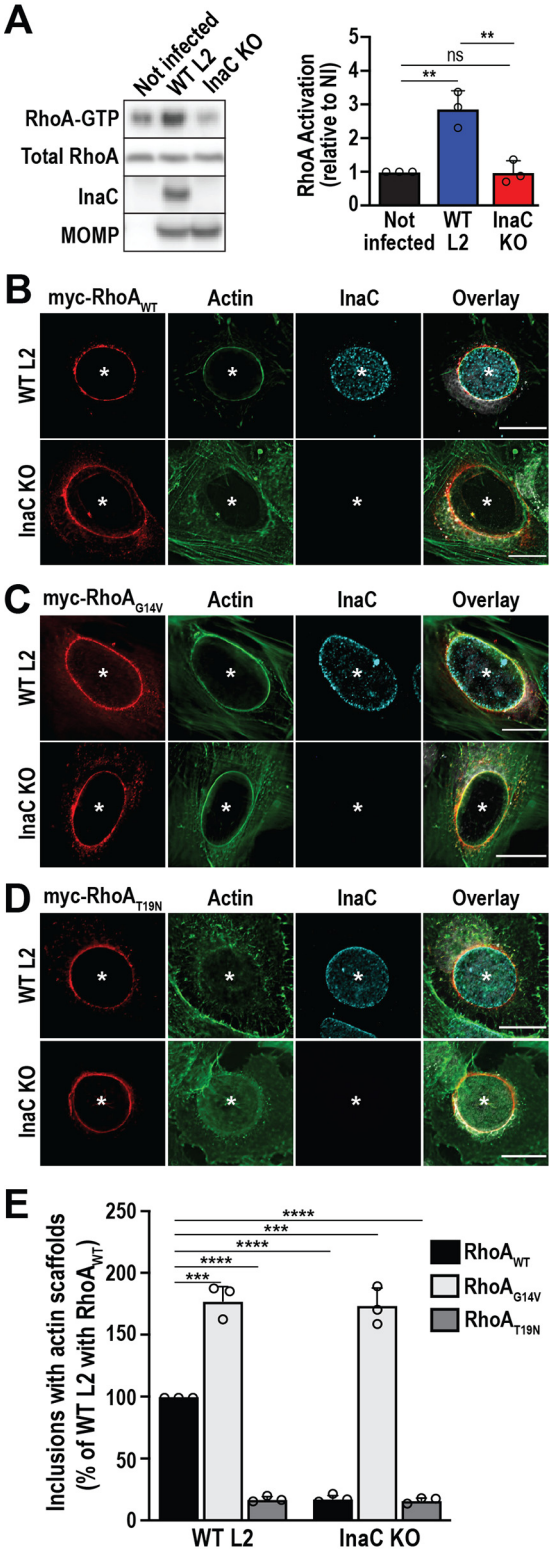

FIG 2 The chlamydial effector InaC is required for the activation of RhoA. (A) HeLa cells were infected with the indicated *C. trachomatis* L2 strains (MOI of 1) for 32 h. RhoA-GTP was isolated as described in Fig. 1C. In the Western blot, anti-InaC antibody confirms the loss of InaC in the InaC KO strain and anti-MOMP antibody confirms infection. The graph denotes the average fold change in RhoA-GTP compared to the uninfected control ± the standard deviation from 3 independent experiments. **, $P < 0.01$; ns, not significant. (B to D) RhoA KO cells were infected with WT or InaC KO *C. trachomatis* L2 (MOI of 2) and transfected with myc-RhoA$_{WT}$ (B), myc-RhoA$_{G14V}$ (C), or myc-RhoA$_{T19N}$ (D) DNA at 4 hpi. Cells were fixed at 38 hpi and labeled with phalloidin (green), anti-myc

(Continued on next page)

at 72 hpi (Fig. 3B). InaC KO inclusions were stabilized when InaC-FLAG was reintroduced on a plasmid (see Fig. S5A and C in the supplemental material). As expected, the complementation of InaC expression also rescued the loss of actin scaffolds (Fig. S5B). Overall, this indicates that InaC is critical for the maintenance of inclusion stability.

To specifically test the impact of the loss of actin scaffolds on inclusion stability, RhoA KO cells were infected with WT *C. trachomatis* L2, and inclusion lysis was measured at 72 hpi as it corresponds to maximal caspase 3/7 activation (Fig. 3B). As controls, we infected RhoA KO cells with InaC KO *C. trachomatis* L2 and treated WT *C. trachomatis* L2-infected cells with latrunculin B to depolymerize all host cell actin. Consistent with previous reports (19), latrunculin B treatment increased levels of inclusion lysis [Fig. 3C, WT L2, (Lat)]. Compared to control cells, inclusion lysis increased by ~15% in the absence of RhoA (Fig. 3C, Ctrl-WT L2 versus RhoA KO-WT L2). Control and RhoA KO cells infected with InaC KO *C. trachomatis* L2 showed similar levels of inclusion lysis to RhoA KO cells infected with WT *C. trachomatis* L2, indicating that InaC and RhoA function in the same pathway to control inclusion stability (Fig. 3C, Ctrl InaC KO versus RhoA KO WT L2). These results suggest that actin scaffolds, but not PTM-MT scaffolds, generated through an InaC-RhoA-dependent pathway specifically contribute to the stability of inclusions during infection.

The presence of RhoA inhibits the formation of PTM-MT scaffolds during infection. PTM-MT scaffolds around the inclusion are most evident around 24 hpi, whereas the formation of actin scaffolds around the inclusion begins later, around 32 hpi (15, 19). Furthermore, actin scaffolds do not form in the absence of RhoA, and PTM-MT scaffolds are disorganized in the absence of ARF1. These data suggest that these two cytoskeletal pathways are independent of each other and are controlled by their corresponding small GTPase. This concept is supported by the fact that each GTPase is activated at specific times during infection: 16 hpi for ARF1 (see Fig. S6 in the supplemental material) and 32 hpi for RhoA (Fig. 1C). Yet, the requirement for the chlamydial protein InaC to control both cytoskeletal events indicates that some degree of cross talk likely exists between these two pathways. Since the inclusion is a fundamental component of *Chlamydia* pathogenicity, this cross talk may allow InaC to finely control the activation/inactivation of each pathway to appropriately time Golgi repositioning and inclusion stability. In this case, we would expect that altering the expression level and/or activity level of either GTPase would impact the formation of the other cytoskeletal element.

To test this hypothesis, we first investigated the impact of RhoA depletion on the formation of PTM-MTs during infection. RhoA KO cells were infected with WT *C. trachomatis* L2, and the PTM-MT scaffolds around the inclusion at 24 hpi were monitored using immunofluorescence microscopy. As expected, PTM-MT scaffolds still assemble around the inclusion in the absence of RhoA, demonstrating that RhoA is not required for their formation (Fig. 4A and B). However, we observe increases of 48% ± 8.8% and 28% ± 7.4% of detyrosinated and acetylated α-tubulin scaffolds, respectively, compared to control cells (Fig. 4A and B, graphs). This enhanced formation of PTM-MT scaffolds is suppressed to WT levels when myc-$RhoA_{WT}$ is expressed in RhoA KO cells, confirming that the phenotype is specifically due to the loss of RhoA (Fig. 4A and B, $RhoA_{WT}$). Furthermore, the expression of either active or inactive RhoA mutants in RhoA KO cells suppresses the enhanced formation of PTM-MTs similarly to myc-$RhoA_{WT}$ (see Fig. S7 in the supplemental material). These results indicate that this phenomenon is due to the presence of RhoA rather than a specific nucleotide-bound state. Altogether, these data suggest that the absence of RhoA enhances the formation of PTM-MTs.

FIG 2 Legend (Continued)
antibody (red), and anti-InaC antibody (cyan). Asterisks denote inclusions. Scale bar, 20 μm. Results are representative of at least 3 independent experiments. (E) The graph displays the average percentage of inclusions with actin scaffolds ± the standard deviation from 3 independent experiments. Data are normalized to cells infected with WT *C. trachomatis* L2 and transfected with myc-$RhoA_{WT}$ DNA. A minimum of 100 inclusions was counted for each condition per experiment. ***, $P < 0.001$; ****, $P < 0.0001$.

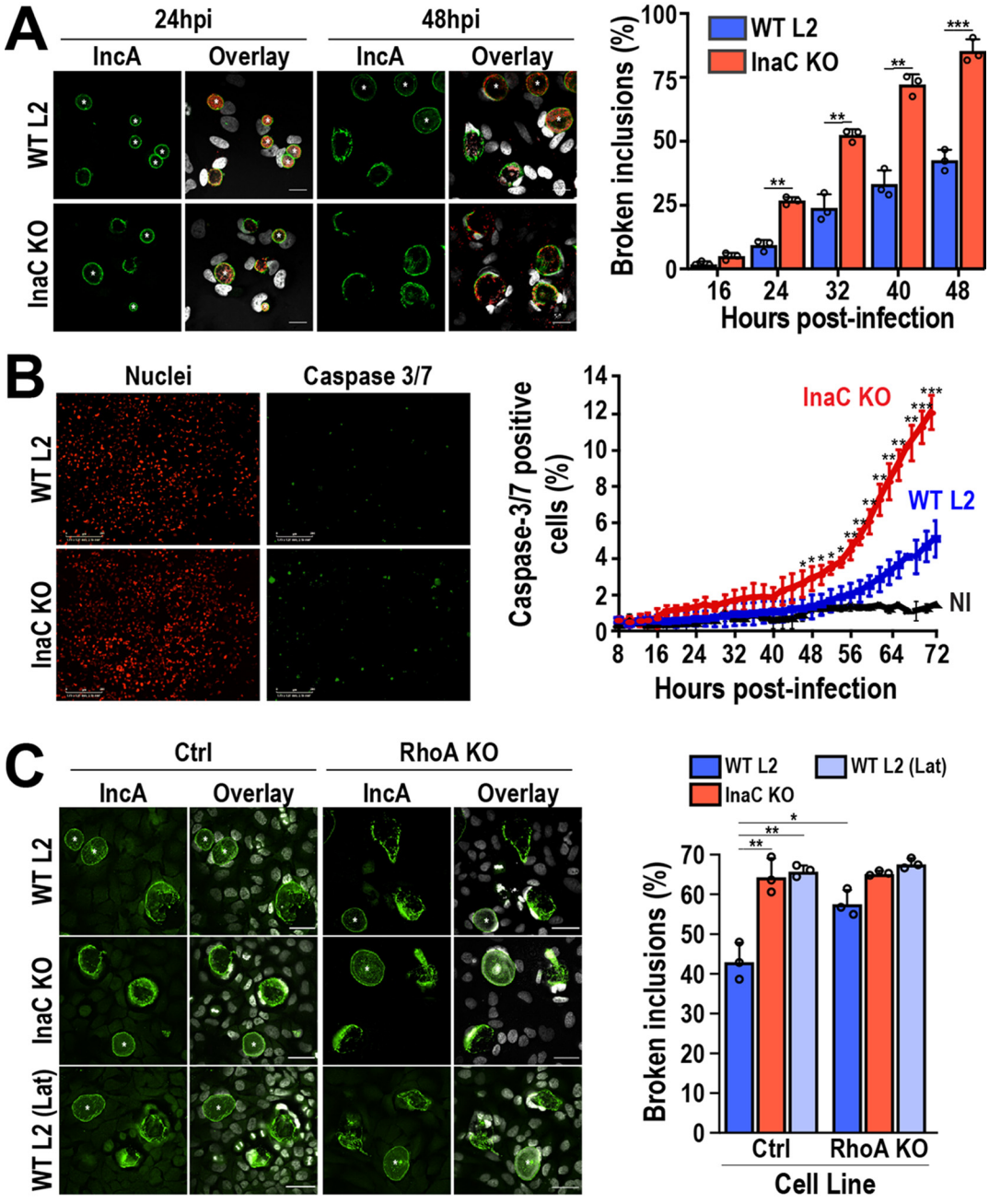

FIG 3 InaC-mediated cytoskeletal pathways contribute to the stability of chlamydial inclusions. (A) HeLa cells were infected with WT or InaC KO *C. trachomatis* L2 (MOI of 0.5) and fixed at the indicated times postinfection. Cells were labeled with anti-IncA antibody (green) to label the inclusion membrane and anti-MOMP antibody (red). Hoechst was used to label DNA (gray). Asterisks denote intact inclusions. Scale bar, 10 μm. The adjacent graph represents the average percentage of broken inclusions at the indicated time points from 3 independent experiments ± the standard deviation. **, $P < 0.01$; ***, $P < 0.001$. (B) Nuclight Red HeLa cells were infected with WT or InaC KO *C. trachomatis* L2 (MOI of 1) for 6 h before the addition of IncuCyte caspase 3/7 green dye for apoptosis at a final concentration of 5 μM. The cells were then imaged every 2 h until 72 hpi on an IncuCyte Zoom imaging system. Nuclei of HeLa cells are shown in red, and caspase 3/7 puncta are shown in green. Scale bar, 300 μm. The graph depicts the average percentage of caspase 3/7-positive cells from 4 independent experiments ± the standard deviation. A minimum of 100 inclusions was counted for each condition. NI, not-infected cells. *, $P < 0.05$; **, $P < 0.01$; ***, $P < 0.001$. (C) Control and RhoA KO HeLa cells were infected with WT or InaC KO *C. trachomatis* L2 (MOI of 0.5) and fixed at 72 hpi. As a control, one set of WT *C. trachomatis* L2-infected cells was treated with 0.5 μM latrunculin B or ethanol (vehicle control) in cell culture medium for 30 min at 37°C 5 h prior to fixation. Vehicle and latrunculin B were washed out with cell culture medium, and the cells were fixed at 72 hpi. Cells were labeled with anti-IncA antibody (green) to label the inclusion membrane and Hoechst (gray) to stain DNA. Scale bar, 40 μm. Asterisks denote intact inclusions. WT L2 (Lat), latrunculin B-treated cells. The graph depicts the average percentage of broken inclusions from 3 independent experiments ± the standard deviation. A minimum of 100 inclusions was counted for each condition. *, $P < 0.05$; **, $P < 0.01$; ***, $P < 0.001$.

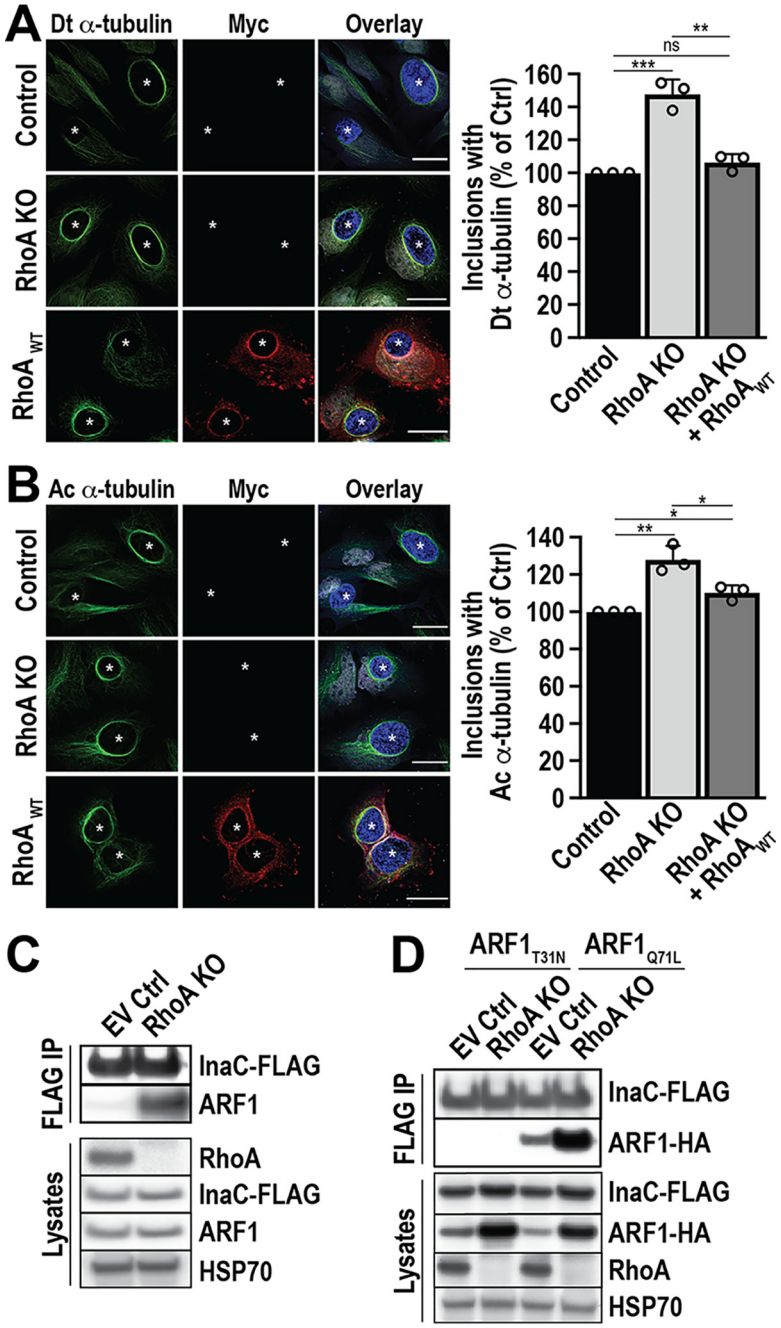

FIG 4 The formation of PTM-MT scaffolds during infection is enhanced in the absence of RhoA. (A and B) Control and RhoA KO HeLa cells were infected with WT *C. trachomatis* L2 (MOI of 2) and transfected with empty vector or myc-RhoA$_{WT}$ DNA at 4 hpi. Cells were fixed at 24 hpi and labeled with anti-detyrosinated α-tubulin (Dt α-tubulin) (A, green), anti-acetylated α-tubulin (Ac α-tubulin) (B, green), anti-myc (red), and anti-MOMP (blue) antibodies. Scale bar, 30 μm. The graphs represent the average percentage of inclusions with Dt α-tubulin (A) or Ac α-tubulin (B) scaffolds normalized to infected control HeLa cells. A minimum of 100 inclusions was counted for each condition per experiment. *, $P < 0.05$; **, $P < 0.01$; ***, $P < 0.001$; ns, not significant. (C) Control and RhoA KO HeLa cells were infected with InaC-FLAG-overexpressing *C. trachomatis* L2 (MOI of 5) and treated with 5 ng/ml anhydrotetracycline (aTc) 4 hpi to induce InaC-FLAG expression. Cells were lysed at 24 hpi, and InaC-FLAG was immunoprecipitated using an anti-FLAG antibody. ARF1 binding was assessed with anti-ARF1 antibody. Lysates were analyzed as a control. Anti-RhoA antibody confirms the loss of RhoA in the RhoA KO. HSP70 served as a loading control. Results are representative of 2 independent experiments. (D) Control and RhoA KO HeLa cells were infected with InaC-FLAG-overexpressing *C. trachomatis* L2 (MOI of 5) and transfected with ARF1$_{T31N}$-HA or ARF1$_{Q71L}$-HA at 4 hpi. InaC-FLAG expression was induced with 5 ng/ml aTc 4 hpi. Cells were lysed at 24 hpi, and InaC-FLAG was immunoprecipitated using anti-FLAG antibody. ARF1 binding was assessed with anti-HA antibody. Lysates were analyzed as a control. Anti-RhoA antibody confirms the loss of RhoA in the RhoA KO. HSP70 served as a loading control. Results are representative of 2 independent experiments.

Since ARF1 is a critical factor in forming PTM-MT scaffolds (15), the enhancement of PTM-MT scaffolds in the RhoA KO could be due to increased complex formation between InaC and ARF1 and/or increased ARF1 activation. To test both possibilities, we infected RhoA KO cells with *C. trachomatis* L2 expressing InaC-FLAG. We then assessed the interactions between InaC-FLAG and endogenous ARF1 compared to the complex formed in control cells. As shown in Fig. 4C, we observe a striking increase in ARF1 binding to InaC-FLAG in the absence of RhoA at 24 hpi. Next, we tested whether the enhanced interaction between ARF1 and InaC is with active or inactive ARF1. Control and RhoA KO cells were transfected with either GDP-bound ($ARF1_{T31N}$-HA [hemagglutinin]) or GTP-bound ($ARF1_{Q71L}$-HA) ARF1 (15, 28) at 3 to 4 hpi with *C. trachomatis* L2 expressing InaC-FLAG. InaC was immunoprecipitated using an anti-FLAG antibody, and the immunoprecipitates were analyzed by Western blotting to identify which ARF1 mutant was bound. As shown in Fig. 4D, only $ARF1_{Q71L}$-HA binds to InaC. The interaction with ARF1-Q71L and InaC is enhanced in the absence of RhoA, demonstrating that the lack of RhoA results in an increase in InaC:ARF1-GTP binding and consequently PTM-MT scaffold formation.

Activation of ARF1 impairs RhoA-GTP-dependent actin scaffold formation. The recruitment of RhoA to the inclusion begins around 24 hpi (Fig. S2). During this time, ARF1 is already activated, and PTM-MT scaffolds are forming. Since (i) the absence of RhoA concomitantly leads to the loss of actin scaffolds and enhances the interaction between ARF1-GTP and InaC (Fig. 4D) and (ii) ARF1 is not required for the formation of actin scaffolds (see Fig. S8 in the supplemental material), we hypothesized that the deactivation of ARF1 might be required for the subsequent downstream activation of RhoA and the formation of actin scaffolds. To test this hypothesis, we expressed the constitutively active $ARF1_{Q71L}$-HA and dominant-negative $ARF1_{T31N}$-HA mutants at 3 to 4 hpi with WT *C. trachomatis* L2 and assessed the formation of actin scaffolds at 32 hpi. Interestingly, the constitutive activation of ARF1 drastically reduces actin scaffold formation by 45% (Fig. 5A and B, $ARF1_{Q71L}$-HA). This effect is specific to the active form of ARF1, as the expression of GDP-bound ARF1 does not influence actin scaffold formation (Fig. 5A and B, $ARF1_{T31N}$-HA).

Next, we determined whether the constitutive activation of ARF1 blocks the activation of RhoA. As shown in Fig. 5C, the activation of RhoA is inhibited by 68% $\pm$ 22% in cells expressing $ARF1_{Q71L}$-HA compared to cells transfected with $ARF1_{WT}$-HA. Collectively, these data demonstrate that cross talk between ARF1 and RhoA is critical for the coordination of PTM-MT and actin scaffolds during *C. trachomatis* infection.

Together, our data support a model in which *Chlamydia* uses a single effector to coordinate two small GTPases and regulate critical cytoskeletal pathways necessary for its survival (Fig. 6). Specifically, ARF1 is activated midcycle (~16 hpi) in an InaC-dependent manner. At this time, RhoA is absent from the inclusion, leaving ARF1 activation unimpeded. As a result, ARF1-GTP actively drives the formation of PTM-MTs. In turn, PTM-MT scaffolds coordinate Golgi rearrangement around the inclusion, which contributes to inclusion growth (15). Around 24 hpi, RhoA starts to relocate to the inclusion membrane. The presence of RhoA blocks ARF1 activation and the generation of additional PTM-MTs. Simultaneously, ARF1-GTP inhibits actin scaffold formation by interfering with RhoA activation. As the infection progresses, the concentration of RhoA on the inclusion membrane increases, further inhibiting ARF1 activation. As ARF1 returns to its inactive GDP-bound state, it can no longer block RhoA activation. The InaC-dependent activation of RhoA fully engages, peaking at 32 hpi and maximizing actin polymerization around the inclusion. As a result, *Chlamydia*'s infectious niche, which has grown significantly due to the continuous supply of lipids from Golgi ministacks, is now fortified against premature lysis and ultimately provides a safe space for RBs to differentiate into infectious EBs and perpetuate the infectious cycle.

DISCUSSION

Here, we have identified a virulence pathway in which the bacterial pathogen *Chlamydia trachomatis* uses a single chlamydial effector to integrate ARF1 and RhoA

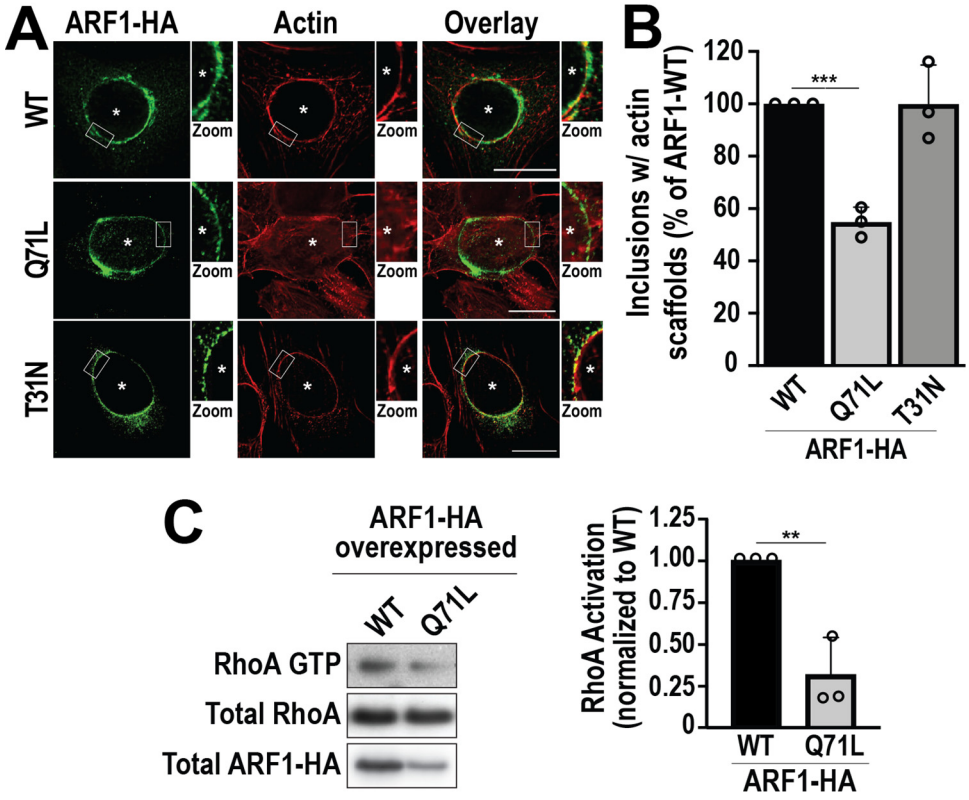

FIG 5 Activation of ARF1 impairs RhoA-GTP-dependent actin scaffold formation. (A) HeLa cells were infected with WT *C. trachomatis* L2 (MOI of 2) and transfected with $ARF1_{WT}$-HA, $ARF1_{Q71L}$-HA, or $ARF1_{T31N}$-HA DNA at 4 hpi. Cells were fixed at 32 hpi and labeled with anti-HA antibody (green) and phalloidin (red). Asterisks denote inclusions. Scale bar, 20 μm. The white box indicates the magnified area shown to the right of the image (Zoom). (B) The graph depicts the average percentage of inclusions with actin scaffolds from 3 independent experiments $\pm$ the standard deviation. Data are normalized to cells transfected with $ARF1_{WT}$-HA DNA. A minimum of 100 inclusions was counted for each condition from 3 independent experiments. ***, $P < 0.001$. (C) HeLa cells were infected with WT *C. trachomatis* L2 (MOI of 1) and transfected with $ARF1_{WT}$-HA or $ARF1_{Q71L}$-HA DNA at the time of infection. The levels of RhoA-GTP were determined as described in Fig. 1C. The graph depicts the average fold change of RhoA-GTP normalized to ARF_{WT}-HA expressing cells from 3 independent experiments $\pm$ the standard deviation. **, $P < 0.01$.

cross talk to precisely time the formation of PTM-MT and actin scaffolds (Fig. 6). Many other intracellular pathogens also target GTPases (29) and integrate GTPase cross talk into their virulence systems. An example is the effector protein EspG expressed by enteropathogenic *E. coli* OH157:H7, which disrupts ER-to-Golgi trafficking by linking ARF1-specific vesicular trafficking events to Rab1 inactivation (30, 31). EspG also blocks phagocytosis by interacting with ARF1 to prevent Rac1 activation and consequently the polymerization of actin at the plasma membrane (32). In contrast, *Salmonella enterica* co-opts an ARF6-ARF1-Rac1 axis to drive plasma membrane ruffling required for entry (33). The *Chlamydia* virulence pathway is most similar to that utilized by *Salmonella* since *Chlamydia* activates rather than inhibits the ARF1-RhoA network to promote successful infection. In this pathway, both RhoA and ARF1 elegantly fine-tune their activity by generating simultaneous feedback loops. The activation of ARF1 prevents the activation of RhoA, while the presence of RhoA downregulates ARF1 activation. While GTPases are well known to regulate each other (34–37), how RhoA and ARF1 influence the function of each other is unknown. Furthermore, whether this process requires other bacterial factors or is an inherent property of these GTPases and their respective effector proteins is under investigation.

Since GTPases are critical components of host signaling networks, manipulating their function or activity can have detrimental consequences for the host. In particular, dysregulation of GTPases involved in coordinating the host cytoskeleton has been linked to cancer hallmarks, such as uncontrolled cell proliferation, migration, and

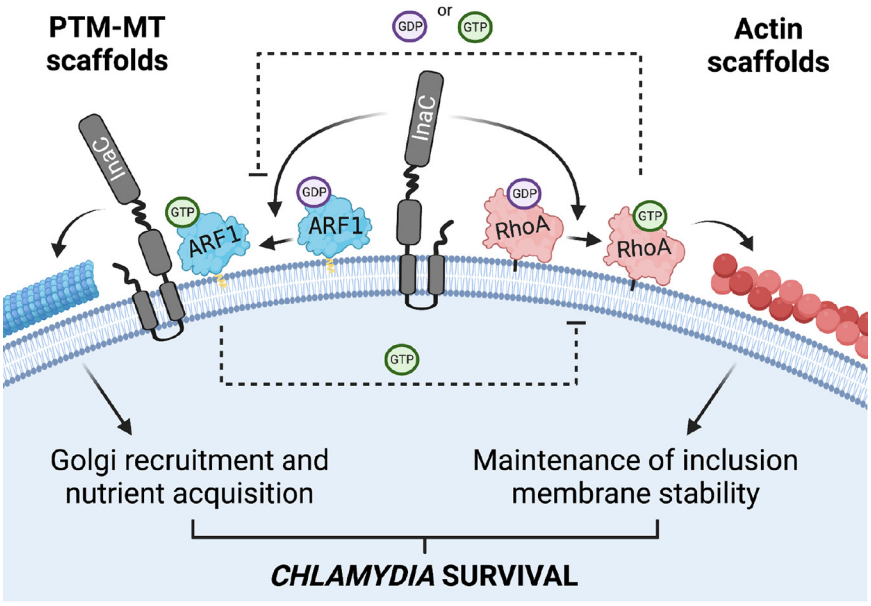

FIG 6 Model of cytoskeletal cross talk during *Chlamydia* infection. *Chlamydia trachomatis* expresses the inclusion membrane protein InaC on the surface of its inclusion facing the host cytosol. InaC is required to activate the host GTPases ARF1 and RhoA on the inclusion membrane and, consequently, for the formation of both PTM-MT and actin scaffolds, respectively. Both PTM-MT and actin scaffolds are essential for *Chlamydia* development and survival. ARF1-GTP is involved in the posttranslational modification of MT scaffolds around the inclusion, which supports Golgi recruitment and nutrient acquisition. ARF1 activation peaks early during infection. As RhoA begins to accumulate on the inclusion ~24 hpi, its presence locally inhibits ARF1 activation and prevents the formation of additional PTM-MTs. Simultaneously, the presence of ARF1-GTP prevents the activation of RhoA and the formation of actin scaffolds early during infection. As ARF1 becomes deactivated and RhoA-GTP reaches its maximum, the formation of actin scaffolds begins. The continual presence of RhoA prevents PTM-MT scaffolds from unnecessarily forming late during infection. The accumulation of actin scaffolds around the inclusion ensures the maximal stability of the inclusion membrane. Figure created with BioRender.com.

differentiation (38, 39). ARF1 and RhoA have been implicated in some aspects of cancer development, including tumor cell invasion and proliferation (40–45). Given that *Chlamydia* infection has been associated with an increased risk for developing cervical and ovarian cancers (46–48), it would be interesting to determine whether the activation of the ARF1-RhoA signaling axis contributes to the potentiation of cancer development in those with a history of chronic *Chlamydia* infection.

As an absolute intracellular bacterium, *Chlamydia* must ensure the integrity of its intracellular niche to establish a successful infection. As *Chlamydia* replicates inside the inclusion, this bacterial compartment matures and expands to eventually occupy most of the host cytoplasm (49). We have previously shown that InaC KO *Chlamydia* displays smaller inclusions and is replication deficient (15). These defects may be due to a combination of factors. (i) They may be a consequence of reduced PTM-MT scaffold formation, which impairs the recruitment of Golgi ministacks around the inclusion that play a role in lipid acquisition and inclusion development (50). (ii) Premature lysis could result in the release of *Chlamydia* into the cytoplasm before the cells have successfully differentiated from RBs into infectious EBs. We show here that InaC KO inclusions lyse significantly earlier than their WT counterparts (Fig. 3A). Since the infected cells then undergo more cell death (Fig. 3B) due to cytoplasmic *Chlamydia*, the bacterium reaches an impasse. While both possibilities likely contribute to the survival of *Chlamydia*, our data demonstrate that the chlamydial effector protein InaC is critical for the protection of *Chlamydia*'s intracellular niche and successful infection by controlling two cytoskeletal networks.

InaC is required to activate both ARF1 and RhoA, which is tightly regulated during *Chlamydia* infection (Fig. 2) (15). This suggests that InaC may possess intrinsic GEF activity. However, we have shown that InaC does not exhibit GEF activity *in vitro* (15),

indicating that other factors likely activate ARF1 and RhoA. How these GTPases are being inactivated and how this inactivation is coordinated are also unknown. Due to the significant number of ARF1 and RhoA GEFs and GTPase-activating proteins (GAPs) (51, 52), it is challenging to postulate what specific regulators may be involved. Nevertheless, GEFs containing GAP domains (52), or GAPs that have both ARF and RhoA GAP domains (53), may be critical for coupling the activities of ARF1 and RhoA.

Our data demonstrate that PTM-MT and actin scaffold formation occurs with distinct kinetics and that disruption of one of these pathways impacts the other. For example, we show that the constitutive activation of ARF1 blocks the formation of actin scaffolds (Fig. 5). Why can't actin scaffolds form in the presence of PTM-MT scaffolds? One possibility is steric hindrance. Since PTM-MTs woven around the inclusion possess enhanced stability and rigidity, the presence of these cytoskeletal elements might limit access to the inclusion membrane either for actin effectors to interact with chlamydial effectors or for the polymerization of actin itself. Additionally, PTM-MT and actin scaffolds may share critical components for their formation. We have already identified InaC as such a regulator; however, other host effectors may also be shared between these two pathways. For example, host formins control the generation of PTM-MTs and the polymerization of actin filaments (54). Thus, the activation of ARF1-dependent PTM-MTs may sequester critical components away from the actin pathway until ARF1 is inactivated, and these effectors can then participate in RhoA-dependent actin scaffold formation. Identification of these components will provide insight into how *Chlamydia* coordinates the specific kinetics of each of these cytoskeletal scaffolds.

While the activation of ARF1 blocks actin scaffold formation, the loss of RhoA results in the enhanced interaction between ARF1 and InaC and increased PTM-MT scaffold formation (Fig. 4). This phenotype can be reversed by the expression of RhoA in any of its nucleotide-bound states (Fig. 4; Fig. S7). The nucleotide independence of this complementation suggests that (i) the presence of RhoA on the inclusion is sufficient to downregulate ARF1 or (ii) RhoA may interact with effectors irrespective of its nucleotide-bound state to shut off ARF1. Several reports have documented that RhoA and other GTPases interact with other proteins in a nucleotide-independent manner to control their localization and activation (55–57). Thus, not only has *Chlamydia* co-opted two host GTPases to coordinate the formation of two cytoskeletal scaffolds, but it has also taken advantage of both nucleotide-dependent and -independent functions of these GTPases.

In summary, our findings have revealed a mechanism by which *Chlamydia* utilizes a single effector protein to control two cytoskeletal pathways. By employing GTPase cross talk, *Chlamydia* temporally regulates the assembly of PTM-MT and actin scaffolds around its inclusion to maintain its parasitic niche. Ultimately, identifying the molecular players participating in these pathways will uncover new targets to combat *Chlamydia trachomatis* infection.

MATERIALS AND METHODS

Cell culture and transfections. HeLa cells (CCL-2; ATCC) and Nuclight Red HeLa cells (Essen Biosciences) were cultured as described previously in Dulbecco's modified Eagle's medium (DMEM) containing 10% fetal bovine serum (FBS), 10 μg/ml gentamicin, and nonessential amino acids (15). Cells were transfected with Continuum transfection reagent (Gemini Bioproducts) using 25 to 50 ng of DNA according to the manufacturer's instructions. For siRNA transfections, HeLa cells were transfected using 25 nM siRNA and DharmaFect 1 reagent (Horizon) according to the manufacturer's instructions 48 h before infection. SmartPool ON-TARGETplus human ARF1 and nontargeting control siRNA were purchased from Dharmacon (15).

***Chlamydia* strains.** Wild-type *Chlamydia trachomatis* serovar L2 (LGV 434/Bu) and InaC KO L2 were obtained from Ted Hackstadt (NIH, Rocky Mountain Laboratories) (15). *C. trachomatis* L2 was propagated and density gradient purified as described preiously (58, 59). The InaC KO and InaC-FLAG *C. trachomatis* L2 strains were generated previously (15, 60). InaC-FLAG-expressing InaC KO *C. trachomatis* L2 was produced by transforming InaC KO *C. trachomatis* L2 with InaC-FLAG pBomb4S-Tet encoding InaC-FLAG under the control of a tetracycline promoter as previously described (15).

Recombinant DNA and cloning. PCR and cloning were conducted using standard procedures. $ARF1_{WT}$-HA and $ARF1_{Q71L}$-HA were generated as previously described (15). $ARF1_{T31N}$-HA was made by PCR amplification of $ARF1_{T31N}$ (J. Keen, Thomas Jefferson University) and ligation into pcDNA3.1(+) containing a C-terminal HA tag. myc-$RhoA_{WT}$ was amplified and ligated into pRK5 containing an N-terminal myc tag. myc-$RhoA_{G14V}$ and myc-$RhoA_{T31N}$ were generated using QuikChange PCR (Agilent) according to the manufacturer's instructions. InaC-FLAG pBomb4S-Tet was generated by exchanging the green fluorescent protein (GFP) cassette in CT813-FLAG pBomb4-Tet (15) with a spectinomycin resistance cassette.

Antibodies. The following primary antibodies were used: anti-HA (chicken, A190-106A; Bethyl Laboratories), anti-actin (rabbit, A2066; Sigma), anti-myc (mouse, 9E10 clone; Juan Bonifacino, NIH), anti-myc (rabbit, 2278; Cell Signaling), anti-RhoA (mouse, ARH04; Cytoskeleton), anti-RhoA (mouse, SAB1400017; Sigma), anti-FLAG (mouse, F1804; Sigma), anti-FLAG (rabbit, 600-401-383; Rockland Immunochemical), anti-ARF1 (mouse, sc-53168; SCBT), anti-α-tubulin (mouse, T5168; Sigma), anti-acetylated α-tubulin (mouse, T6793; Sigma), anti-detyrosinated α-tubulin (rabbit, 48389; Abcam), ActiStain-488 (PHDG1; Cytoskeleton), Actistain-555 (PHDH1-A; Cytoskeleton), anti-heat shock protein 70 (HSP70) (chicken, SPC-178D; StressMarq), anti-InaC (mouse; T. Hackstadt), anti-IncA (rabbit; T. Hackstadt), and anti-MOMP (goat, 1621; ViroStat). The following secondary reagents were used: Hoechst dye (H1399) and goat and donkey anti-mouse, anti-goat, anti-rabbit, and anti-chicken (IgY) IgG Alexa Fluor 488-, 555-, or 647-conjugated secondary antibodies (Invitrogen). Donkey anti-chicken, anti-mouse, or anti-rabbit IgG and IgY horseradish peroxidase (HRP)-conjugated secondary antibodies were purchased from Invitrogen.

Generation and characterization of the RhoA KO CRISPR/Cas9 cell line. Guide RNAs targeting human RhoA was designed using the sequences available in GenBank and analyzed for their efficiency and off-target effects, using the CRISPOR (61) and the Broad Institute single guide RNA (sgRNA) designer (62) databases with default cutoffs. The optimal guide RNA was prepared by annealing primers FO1033 (5′-CAC CGG AAC TAT GTG GCA GAT ATC G-3′) and FO1034 (5′-AAA CCG ATA TCT GCC ACA TAG TTC C-3′). The guide RNA was then inserted into the BsbI site of the pSpCas9(BB)-2A-GFP (PX458) vector (S. Kim, Thomas Jefferson University) and confirmed by Sanger sequencing (Genewiz). HeLa cells were then transfected with pSpCas9(BB)-2A-GFP containing the guide RNA as well as the empty vector (no guide RNA) as described previously (63). Individual clones were isolated by limited dilution. Successful knockout of RhoA was confirmed by Western blotting. Cell division analysis using carboxyfluorescein succinimidyl ester (CFSE) labeling was conducted as described previously (63).

Preparation of cell lysates for Western blot analysis. Cells were washed with PBS and lysed with ice-cold lithium dodecyl sulfate (LDS)-PAGE sample buffer (Invitrogen) containing 250 U/μl benzonase (Accelagen), 1 μg/ml pepstatin A, 5 μg/ml leupeptin, 1 mM phenylmethylsulfonyl fluoride, 10 mM sodium fluoride, and 5.4 mM sodium orthovanadate for 10 min on ice. β-Mercaptoethanol was then added to a final concentration of 0.36 M at 95°C for 5 min, followed by centrifugation at 20,000 $\times$ *g* at 4°C for 10 min. Protein concentrations were determined using the Pierce 660-nm protein assay reagent containing ionic detergent compatibility reagent and read at 660 nm in a SpectraMax M2 plate reader.

Western blotting. Samples were separated on 4- to 12% bis-Tris SDS-PAGE gels (Invitrogen) and transferred to polyvinylidene difluoride membranes for 1 h at 90 V and 4°C in transfer buffer (25 mM Tris, 192 mM glycine, 10% methanol). Membranes were washed in TBS (25 mM Tris base, 150 mM NaCl [pH 7.5]) and then dried at room temperature for 1 h. Membranes were rehydrated with methanol and washed with TBS and TBST (TBS containing 0.1% Tween 20). Membranes were then blocked for 1 h at room temperature with blocking buffer (3% bovine serum albumin and 0.05% sodium azide in TBST). After blocking, membranes were incubated in primary antibody overnight at 4°C in blocking buffer. Membranes were washed with TBST before incubation with HRP-conjugated secondary antibody for 1 h at room temperature in 0.5% milk diluted in TBST. Membranes were then washed several times with TBST and TBS and revealed with SuperSignal West Dura extended duration substrate (Thermo Scientific). Membranes were imaged on a FluorChem R system (ProteinSimple). Band intensities were quantified using AlphaView software (ProteinSimple).

Inclusion lysis analysis. Cells were infected with WT or InaC KO *C. trachomatis* L2 at a multiplicity of infection (MOI) of 0.5 and fixed at the indicated times. When noted, WT *C. trachomatis* L2-infected cells were treated with either 0.5 μM latrunculin B or ethanol (vehicle control) in cell culture medium for 30 min at 37°C 5 h prior to fixation. Latrunculin B and ethanol were washed out with cell culture medium, and cells were fixed at the indicated times. For complementation of inclusion stability, HeLa cells were infected with WT or InaC-FLAG-expressing InaC KO *C. trachomatis* L2 at an MOI of 0.5 and fixed at 48 hpi. Inclusion integrity was determined by labeling inclusions with IncA and identifying discontinuity in the labeling of IncA on the inclusion membrane. An inclusion was considered broken or lysed when one or more substantial gaps in the incidence of IncA labeling were observed using wide-field fluorescence microscopy. Most of the broken inclusions were missing large pieces of the inclusion membrane. When inclusion integrity was less clear, the presence of *Chlamydia* in the cytosol was used to identify a broken inclusion.

Immunofluorescence microscopy. HeLa cells were fixed with either (i) 4% paraformaldehyde in PEMS buffer (80 mM PIPES, 5 mM EDTA, 2 mM $MgCl_2$, 50 mM sucrose [pH 6.8]) for 15 min at room temperature or (ii) ice-cold methanol for 10 min at room temperature. Cells were then washed in IF-G buffer (25 mM HEPES, 150 mM NaCl, 900 nM $CaCl_2$, 500 nM $MgCl_2$, 100 mM glycine [pH 7.5]) for paraformaldehyde fixation or IF buffer (25 mM HEPES, 150 mM NaCl, 900 nM $CaCl_2$, 500 nM $MgCl_2$ [pH 7.5]) for methanol fixation. Permeabilization was performed with 0.2% Triton X-100 in IF buffer for 10 min, followed by washes with 0.1% Triton X-100 in IF buffer. Cells were then blocked for 1 h with either (i) goat serum (10% goat serum, 0.05% sodium azide, 0.1% Triton X-100 in IF buffer) or (ii) donkey serum (10% donkey serum, 0.05% sodium azide, 0.1% Triton X-100 in IF buffer) blocking buffer. After blocking, cells were treated with the primary antibodies diluted in the appropriate blocking buffer for 1 h at room temperature. Cells were washed with 0.1% Triton X-100 in IF buffer and subsequently incubated with Alexa Fluor-conjugated secondary antibodies and Hoechst, diluted in the appropriate blocking buffer for 1 h at room temperature. Cells were washed 0.1% Triton X-100 in IF buffer, followed by multiple washes with IF buffer, and mounted on coverslips with ProLong glass antifade mounting medium (Invitrogen). For inclusion lysis experiments, permeabilization, blocking, and subsequent washes were performed in 0.1% saponin instead of Triton X-100. A minimum of 100 cells per condition were observed and imaged with a 60$\times$ oil immersion lens on a Nikon TiE inverted fluorescence microscope and Elements software (Nikon). Images were processed using ImageJ (NIH).

ARF1 and RhoA activation assays. Cells were seeded at a density of 2.9×10^6 cells per 150-mm tissue culture dish 24 h before infection with the indicated strains at an effective MOI of 1. Each plate of cells was lysed at 24 hpi (for ARF1) or 32 hpi (for RhoA) in 700 μl of 2× lysis buffer (50 mM Tris, 10 mM $MgCl_2$, 0.5 M NaCl, 2% Igepal [pH 7.5]) containing protease inhibitor cocktail (K1007; APExBio) and immediately clarified by centrifugation at 20,000 × *g* for 1 min at 4°C. Lysates were rapidly frozen in liquid nitrogen and stored at −80°C. Isolation of ARF1-GTP was performed as described previously (15), using GST-GGA1 agarose and 800 μg of cell lysate diluted to 1× lysis buffer using distilled water. RhoA-GTP was isolated using a similar protocol, except the GST-GGA1 was replaced with the GST-Rhotekin RBD agarose beads (BK036; Cytoskeleton). The amount of active GTPase was determined by dividing the ARF1-GTP or RhoA-GTP signal from the pulldown with the ARF1 or RhoA signal from the cell lysate (total GTPase).

Immunoprecipitation. Prior to lysis, cells were fixed in 0.6% paraformaldehyde for 20 min at 4°C. Fixed cells were quenched with multiple washes in IF-G buffer. HeLa cells were lysed in ice-cold lysis buffer as described previously (15). Lysates were clarified by centrifugation, and equal amounts of protein were incubated overnight at 4°C with an anti-FLAG or anti-myc antibody immobilized on protein G Plus agarose beads. The beads were washed with lysis buffer and boiled at 95°C for 5 min in NuPAGE LDS sample buffer (Invitrogen). All samples were analyzed by Western blotting.

Caspase 3/7 assay. IncuCyte HeLa Nuclight Red cells (Essen Biosciences) were seeded into 96-well plates at a density of 7.5×10^3 cells per well 24 h before infection with WT *C. trachomatis* L2 or InaC KO *C. trachomatis* L2 at an MOI of 1. The infection was synchronized by centrifugation at 1,000 × *g* for 1 h at room temperature. At 6 hpi, the IncuCyte caspase 3/7 green dye for apoptosis (Essen Biosciences) was added to each well at a final concentration of 5 μM. Wells were imaged every 2 h until 72 hpi using an IncuCyte Zoom imaging system (Essen Biosciences). The percentage of caspase 3/7-positive cells was calculated by dividing the number of caspase 3/7 puncta by the number of red nuclei.

Statistical analysis. A two-tailed Student's *t* test was employed when comparing the means from two independent groups. GraphPad Prism 9 was used for all statistical testing and data analysis. *P* values of <0.05 were considered statistically significant.

Data availability. The authors declare that all other relevant data supporting the findings of this study are included in the manuscript and its supplemental files or from the corresponding author upon request.

SUPPLEMENTAL MATERIAL

Supplemental material is available online only.

FIG S1, PDF file, 0.7 MB.

FIG S2, PDF file, 4.8 MB.

FIG S3, PDF file, 3 MB.

FIG S4, PDF file, 5.7 MB.

FIG S5, TIF file, 2.6 MB.

FIG S6, PDF file, 0.1 MB.

FIG S7, PDF file, 15.4 MB.

FIG S8, PDF file, 10.9 MB.

ACKNOWLEDGEMENTS

We thank Christian Xander (UNC, Chapel Hill) and William Foss (Thomas Jefferson University) for their assistance with this project. We also thank Mary Weber (U Iowa) for her assistance in generating the InaC-FLAG-expressing InaC KO L2 strain.

The work reported in this publication was supported by the National Institute of Allergy and Infectious Diseases at the National Institutes of Health under grant R01AI144081 to F.P. A.H. is supported by the Thomas Jefferson University Dean's matching fellowship to the Training Program in Vaccines and Immunotherapies for Infectious Diseases and Cancer (T32AI134646). T.M.-B. was supported by a Ph.D. fellowship (PD/BD/113772/2015) as part of the MD/Ph.D. program of the University of Minho School of Medicine funded by the Fundação para a Ciência e Tecnologia (FCT).

Conceived and designed experiments: A.H., J.W., F.P.; performed the experiments: A.H., J.W., N.M.R., T.M.-B.; analyzed the data: A.H., J.W., F.P.; wrote the paper: A.H., J.W., F.P.

REFERENCES

1. Fletcher DA, Mullins RD. 2010. Cell mechanics and the cytoskeleton. Nature 463:485–492. https://doi.org/10.1038/nature08908.
2. Wesolowski J, Paumet F. 2017. Taking control: reorganization of the host cytoskeleton by Chlamydia. F1000Res 6:2058. https://doi.org/10.12688/f1000research.12316.1.
3. de Souza Santos M, Orth K. 2015. Subversion of the cytoskeleton by intracellular bacteria: lessons from Listeria, Salmonella and Vibrio. Cell Microbiol 17:164–173. https://doi.org/10.1111/cmi.12399.
4. Rottner K, Stradal TE, Wehland J. 2005. Bacteria-host-cell interactions at the plasma membrane: stories on actin cytoskeleton subversion. Dev Cell 9:3–17. https://doi.org/10.1016/j.devcel.2005.06.002.
5. Schachter J, West SK, Mabey D, Dawson CR, Bobo L, Bailey R, Vitale S, Quinn TC, Sheta A, Sallam S, Mkocha H, Mabey D, Faal H. 1999. Azithromycin in control of trachoma. Lancet 354:630–635. https://doi.org/10.1016/S0140-6736(98)12387-5.
6. Belland RJ, Zhong G, Crane DD, Hogan D, Sturdevant D, Sharma J, Beatty WL, Caldwell HD. 2003. Genomic transcriptional profiling of the developmental

cycle of Chlamydia trachomatis. Proc Natl Acad Sci U S A 100:8478–8483. https://doi.org/10.1073/pnas.1331135100.
7. Lane BJ, Mutchler C, Al Khodor S, Grieshaber SS, Carabeo RA. 2008. Chlamydial entry involves TARP binding of guanine nucleotide exchange factors. PLoS Pathog 4:e1000014. https://doi.org/10.1371/journal.ppat.1000014.
8. Jewett TJ, Fischer ER, Mead DJ, Hackstadt T. 2006. Chlamydial TARP is a bacterial nucleator of actin. Proc Natl Acad Sci U S A 103:15599–15604. https://doi.org/10.1073/pnas.0603044103.
9. Jiwani S, Ohr RJ, Fischer ER, Hackstadt T, Alvarado S, Romero A, Jewett TJ. 2012. Chlamydia trachomatis Tarp cooperates with the Arp2/3 complex to increase the rate of actin polymerization. Biochem Biophys Res Commun 420:816–821. https://doi.org/10.1016/j.bbrc.2012.03.080.
10. Carabeo RA, Grieshaber SS, Fischer E, Hackstadt T. 2002. Chlamydia trachomatis induces remodeling of the actin cytoskeleton during attachment and entry into HeLa cells. Infect Immun 70:3793–3803. https://doi.org/10.1128/IAI.70.7.3793-3803.2002.
11. Carabeo RA, Grieshaber SS, Hasenkrug A, Dooley C, Hackstadt T. 2004. Requirement for the Rac GTPase in Chlamydia trachomatis invasion of non-phagocytic cells. Traffic 5:418–425. https://doi.org/10.1111/j.1398-9219.2004.00184.x.
12. Carabeo RA, Dooley CA, Grieshaber SS, Hackstadt T. 2007. Rac interacts with Abi-1 and WAVE2 to promote an Arp2/3-dependent actin recruitment during chlamydial invasion. Cell Microbiol 9:2278–2288. https://doi.org/10.1111/j.1462-5822.2007.00958.x.
13. Al-Younes HM, Al-Zeer MA, Khalil H, Gussmann J, Karlas A, Machuy N, Brinkmann V, Braun PR, Meyer TF. 2011. Autophagy-independent function of MAP-LC3 during intracellular propagation of Chlamydia trachomatis. Autophagy 7:814–828. https://doi.org/10.4161/auto.7.8.15597.
14. Al-Zeer MA, Al-Younes HM, Kerr M, Abu-Lubad M, Gonzalez E, Brinkmann V, Meyer TF. 2014. Chlamydia trachomatis remodels stable microtubules to coordinate Golgi stack recruitment to the chlamydial inclusion surface. Mol Microbiol 94:1285–1297. https://doi.org/10.1111/mmi.12829.
15. Wesolowski J, Weber MM, Nawrotek A, Dooley CA, Calderon M, St Croix CM, Hackstadt T, Cherfils J, Paumet F. 2017. Chlamydia hijacks ARF GTPases to coordinate microtubule posttranslational modifications and Golgi complex positioning. mBio 8:e02280-16. https://doi.org/10.1128/mBio.02280-16.
16. Eshun-Wilson L, Zhang R, Portran D, Nachury MV, Toso DB, Löhr T, Vendruscolo M, Bonomi M, Fraser JS, Nogales E. 2019. Effects of alpha-tubulin acetylation on microtubule structure and stability. Proc Natl Acad Sci U S A 116:10366–10371. https://doi.org/10.1073/pnas.1900441116.
17. Peris L, Wagenbach M, Lafanechère L, Brocard J, Moore AT, Kozielski F, Job D, Wordeman L, Andrieux A. 2009. Motor-dependent microtubule disassembly driven by tubulin tyrosination. J Cell Biol 185:1159–1166. https://doi.org/10.1083/jcb.200902142.
18. Hackstadt T, Rockey DD, Heinzen RA, Scidmore MA. 1996. Chlamydia trachomatis interrupts an exocytic pathway to acquire endogenously synthesized sphingomyelin in transit from the Golgi apparatus to the plasma membrane. EMBO J 15:964–977. https://doi.org/10.1002/j.1460-2075.1996.tb00433.x.
19. Kumar Y, Valdivia RH. 2008. Actin and intermediate filaments stabilize the Chlamydia trachomatis vacuole by forming dynamic structural scaffolds. Cell Host Microbe 4:159–169. https://doi.org/10.1016/j.chom.2008.05.018.
20. Hybiske K, Stephens RS. 2007. Mechanisms of host cell exit by the intracellular bacterium Chlamydia. Proc Natl Acad Sci U S A 104:11430–11435. https://doi.org/10.1073/pnas.0703218104.
21. Aspengren S, Wielbass L, Wallin M. 2006. Effects of acrylamide, latrunculin, and nocodazole on intracellular transport and cytoskeletal organization in melanophores. Cell Motil Cytoskeleton 63:423–436. https://doi.org/10.1002/cm.20134.
22. Kokes M, Dunn JD, Granek JA, Nguyen BD, Barker JR, Valdivia RH, Bastidas RJ. 2015. Integrating chemical mutagenesis and whole-genome sequencing as a platform for forward and reverse genetic analysis of Chlamydia. Cell Host Microbe 17:716–725. https://doi.org/10.1016/j.chom.2015.03.014.
23. Hodge RG, Ridley AJ. 2016. Regulating Rho GTPases and their regulators. Nat Rev Mol Cell Biol 17:496–510. https://doi.org/10.1038/nrm.2016.67.
24. Ren XD, Kiosses WB, Schwartz MA. 1999. Regulation of the small GTP-binding protein Rho by cell adhesion and the cytoskeleton. EMBO J 18:578–585. https://doi.org/10.1093/emboj/18.3.578.
25. Ghosh PM, Ghosh-Choudhury N, Moyer ML, Mott GE, Thomas CA, Foster BA, Greenberg NM, Kreisberg JI. 1999. Role of RhoA activation in the growth and morphology of a murine prostate tumor cell line. Oncogene 18:4120–4130. https://doi.org/10.1038/sj.onc.1202792.
26. Tatsis N, Lannigan DA, Macara IG. 1998. The function of the p190 Rho GTPase-activating protein is controlled by its N-terminal GTP binding domain. J Biol Chem 273:34631–34638. https://doi.org/10.1074/jbc.273.51.34631.
27. Cho SG, Li D, Stafford LJ, Luo J, Rodriguez-Villanueva M, Wang Y, Liu M. 2009. KiSS1 suppresses TNFalpha-induced breast cancer cell invasion via an inhibition of RhoA-mediated NF-kappaB activation. J Cell Biochem 107:1139–1149. https://doi.org/10.1002/jcb.22216.
28. Dascher C, Balch WE. 1994. Dominant inhibitory mutants of ARF1 block endoplasmic reticulum to Golgi transport and trigger disassembly of the Golgi apparatus. J Biol Chem 269:1437–1448. https://doi.org/10.1016/S0021-9258(17)42277-0.
29. Quintero CA, Tudela JG, Damiani MT. 2015. Rho GTPases as pathogen targets: focus on curable sexually transmitted infections. Small GTPases 6:108–118. https://doi.org/10.4161/21541248.2014.991233.
30. Selyunin AS, Reddick LE, Weigele BA, Alto NM. 2014. Selective protection of an ARF1-GTP signaling axis by a bacterial scaffold induces bidirectional trafficking arrest. Cell Rep 6:878–891. https://doi.org/10.1016/j.celrep.2014.01.040.
31. Selyunin AS, Sutton SE, Weigele BA, Reddick LE, Orchard RC, Bresson SM, Tomchick DR, Alto NM. 2011. The assembly of a GTPase-kinase signalling complex by a bacterial catalytic scaffold. Nature 469:107–111. https://doi.org/10.1038/nature09593.
32. Humphreys D, Singh V, Koronakis V. 2016. Inhibition of WAVE regulatory complex activation by a bacterial virulence effector counteracts pathogen phagocytosis. Cell Rep 17:697–707. https://doi.org/10.1016/j.celrep.2016.09.039.
33. Humphreys D, Davidson AC, Hume PJ, Makin LE, Koronakis V. 2013. Arf6 coordinates actin assembly through the WAVE complex, a mechanism usurped by Salmonella to invade host cells. Proc Natl Acad Sci U S A 110:16880–16885. https://doi.org/10.1073/pnas.1311680110.
34. Benink HA, Bement WM. 2005. Concentric zones of active RhoA and Cdc42 around single cell wounds. J Cell Biol 168:429–439. https://doi.org/10.1083/jcb.200411109.
35. Li Z, Aizenman CD, Cline HT. 2002. Regulation of rho GTPases by crosstalk and neuronal activity in vivo. Neuron 33:741–750. https://doi.org/10.1016/S0896-6273(02)00621-9.
36. Ridley AJ, Paterson HF, Johnston CL, Diekmann D, Hall A. 1992. The small GTP-binding protein rac regulates growth factor-induced membrane ruffling. Cell 70:401–410. https://doi.org/10.1016/0092-8674(92)90164-8.
37. Cheng L, Mahon GM, Kostenko EV, Whitehead IP. 2004. Pleckstrin homology domain-mediated activation of the rho-specific guanine nucleotide exchange factor Dbs by Rac1. J Biol Chem 279:12786–12793. https://doi.org/10.1074/jbc.M313099200.
38. Hall A. 2009. The cytoskeleton and cancer. Cancer Metastasis Rev 28:5–14. https://doi.org/10.1007/s10555-008-9166-3.
39. Fife CM, McCarroll JA, Kavallaris M. 2014. Movers and shakers: cell cytoskeleton in cancer metastasis. Br J Pharmacol 171:5507–5523. https://doi.org/10.1111/bph.12704.
40. Boulay P-L, Schlienger S, Lewis-Saravalli S, Vitale N, Ferbeyre G, Claing A. 2011. ARF1 controls proliferation of breast cancer cells by regulating the retinoblastoma protein. Oncogene 30:3846–3861. https://doi.org/10.1038/onc.2011.100.
41. Ridley AJ. 2001. Rho GTPases and cell migration. J Cell Sci 114:2713–2722. https://doi.org/10.1242/jcs.114.15.2713.
42. Gu G, Chen Y, Duan C, Zhou L, Chen C, Chen J, Cheng J, Shi N, Jin Y, Xi Q, Zhong J. 2017. Overexpression of ARF1 is associated with cell proliferation and migration through PI3K signal pathway in ovarian cancer. Oncol Rep 37:1511–1520. https://doi.org/10.3892/or.2017.5388.
43. Zhao LG, Wang J, Li J, Li QF. 2020. miR-744-5p inhibits cellular proliferation and invasion via targeting ARF1 in epithelial ovarian cancer. Kaohsiung J Med Sci 36:799–807. https://doi.org/10.1002/kjm2.12253.
44. Zaoui K, Boudhraa Z, Khalifé P, Carmona E, Provencher D, Mes-Masson A-M. 2019. Ran promotes membrane targeting and stabilization of RhoA to orchestrate ovarian cancer cell invasion. Nat Commun 10:2666. https://doi.org/10.1038/s41467-019-10570-w.
45. Lewis-Saravalli S, Campbell S, Claing A. 2013. ARF1 controls Rac1 signaling to regulate migration of MDA-MB-231 invasive breast cancer cells. Cell Signal 25:1813–1819. https://doi.org/10.1016/j.cellsig.2013.05.011.
46. Koskela P, Anttila T, Bjørge T, Brunsvig A, Dillner J, Hakama M, Hakulinin T, Jellum E, Lehtinin M, Lenner P, Luostarinen T, Pukkala E, Saikku P, Thoreson S, Youngman L, Paavonen J. 2000. Chlamydia trachomatis infection as a risk factor for invasive cervical cancer. Int J Cancer 85:35–39. https://doi.org/10.1002/(sici)1097-0215(20000101)85:1<35::aid-ijc6>3.0.co;2-a.

47. Das M. 2018. Chlamydia infection and ovarian cancer risk. Lancet Oncol 19:e338. https://doi.org/10.1016/S1470-2045(18)30421-2.
48. Trabert B, Waterboer T, Idahl A, Brenner N, Brinton LA, Butt J, Coburn SB, Hartge P, Hufnagel K, Inturrisi F, Lissowska J, Mentzer A, Peplonska B, Sherman ME, Wills GS, Woodhall SC, Pawlita M, Wentzensen N. 2019. Antibodies against Chlamydia trachomatis and ovarian cancer risk in two independent populations. J Natl Cancer Inst 111:129–136. https://doi.org/10.1093/jnci/djy084.
49. Engström P, Bergström M, Alfaro AC, Krishnan KS, Bahnan W, Almqvist F, Bergström S. 2015. Expansion of the Chlamydia trachomatis inclusion does not require bacterial replication. Int J Med Microbiol 305:378–382. https://doi.org/10.1016/j.ijmm.2015.02.007.
50. Heuer D, Rejman Lipinski A, Machuy N, Karlas A, Wehrens A, Siedler F, Brinkmann V, Meyer TF. 2009. Chlamydia causes fragmentation of the Golgi compartment to ensure reproduction. Nature 457:731–735. https://doi.org/10.1038/nature07578.
51. Sztul E, Chen P-W, Casanova JE, Cherfils J, Dacks JB, Lambright DG, Lee F-JS, Randazzo PA, Santy LC, Schürmann A, Wilhelmi I, Yohe ME, Kahn RA. 2019. ARF GTPases and their GEFs and GAPs: concepts and challenges. Mol Biol Cell 30:1249–1271. https://doi.org/10.1091/mbc.E18-12-0820.
52. Bos JL, Rehmann H, Wittinghofer A. 2007. GEFs and GAPs: critical elements in the control of small G proteins. Cell 129:865–877. https://doi.org/10.1016/j.cell.2007.05.018.
53. Miura K, Jacques KM, Stauffer S, Kubosaki A, Zhu K, Hirsch DS, Resau J, Zheng Y, Randazzo PA. 2002. ARAP1: a point of convergence for Arf and Rho signaling. Mol Cell 9:109–119. https://doi.org/10.1016/s1097-2765(02)00428-8.
54. Chesarone MA, DuPage AG, Goode BL. 2010. Unleashing formins to remodel the actin and microtubule cytoskeletons. Nat Rev Mol Cell Biol 11:62–74. https://doi.org/10.1038/nrm2816.
55. Seoh ML, Ng CH, Yong J, Lim L, Leung T. 2003. ArhGAP15, a novel human RacGAP protein with GTPase binding property. FEBS Lett 539:131–137. https://doi.org/10.1016/s0014-5793(03)00213-8.
56. Abdul-Ghani M, Gougeon PY, Prosser DC, Da-Silva LF, Ngsee JK. 2001. PRA isoforms are targeted to distinct membrane compartments. J Biol Chem 276:6225–6233. https://doi.org/10.1074/jbc.M009073200.
57. Gingras D, Gauthier F, Lamy S, Desrosiers RR, Beliveau R. 1998. Localization of RhoA GTPase to endothelial caveolae-enriched membrane domains. Biochem Biophys Res Commun 247:888–893. https://doi.org/10.1006/bbrc.1998.8885.
58. Caldwell HD, Kromhout J, Schachter J. 1981. Purification and partial characterization of the major outer membrane protein of Chlamydia trachomatis. Infect Immun 31:1161–1176. https://doi.org/10.1128/iai.31.3.1161-1176.1981.
59. Furness G, Graham DM, Reeve P. 1960. The titration of trachoma and inclusion blennorrhoea viruses in cell cultures. J Gen Microbiol 23:613–619. https://doi.org/10.1099/00221287-23-3-613.
60. Bauler LD, Hackstadt T. 2014. Expression and targeting of secreted proteins from Chlamydia trachomatis. J Bacteriol 196:1325–1334. https://doi.org/10.1128/JB.01290-13.
61. Haeussler M, Schönig K, Eckert H, Eschstruth A, Mianné J, Renaud J-B, Schneider-Maunoury S, Shkumatava A, Teboul L, Kent J, Joly J-S, Concordet J-P. 2016. Evaluation of off-target and on-target scoring algorithms and integration into the guide RNA selection tool CRISPOR. Genome Biol 17:148. https://doi.org/10.1186/s13059-016-1012-2.
62. Doench JG, Fusi N, Sullender M, Hegde M, Vaimberg EW, Donovan KF, Smith I, Tothova Z, Wilen C, Orchard R, Virgin HW, Listgarten J, Root DE. 2016. Optimized sgRNA design to maximize activity and minimize off-target effects of CRISPR-Cas9. Nat Biotechnol 34:184–191. https://doi.org/10.1038/nbt.3437.
63. Monteiro-Bras T, Wesolowski J, Paumet F. 2019. Depletion of SNAP-23 and Syntaxin 4 alters lipid droplet homeostasis during Chlamydia infection. Microb Cell 7:46–58. https://doi.org/10.15698/mic2020.02.707.